5-2012

Numerical study for a viscoelastic fluid-structure interaction problem

Shuhan Xu
Clemson University, shuhanx@g.clemson.edu

Numerical study for a viscoelastic fluid-structure interaction problem

---

A Dissertation
Presented to
the Graduate School of
Clemson University

In Partial Fulfillment
of the Requirements for the Degree
Master of Science
Mathematical Science

---

by
Shuhan Xu
May 2012

Accepted by:
Dr. Hyesuk Lee, Committee Chair
Dr. Leo Rebholz
Dr. Daniel Warner

Abstract

In this thesis, we consider a viscoelastic flow in a moving domain, which has significant applications in biology and industry. Numerical approximation schemes are developed based on the Arbitrary Lagrangian-Eulerian (ALE) formulation of the flow equations. A spatial discretization is accomplished by the finite element method, and the time descritization is carried by either the implicit Euler method or the Crank-Nicolson method. Numerical results are presented for a fluid in a moving domain, where the boundary movement is specified by a given function. Then, we extend our work to a fluid-structure interaction problem. This system consists of a two-dimensional viscoelastic flow and a one-dimensional structure equation. We show how the system can be split and how each subproblem can be solved using interface conditions. Finally, we present some numerical results for the fluid-structure coupled system.

Contents

Chapter 1

Introduction

Fluid structure interaction problems have various applications in physics and biology. Such problems include simulation of blood flows in vessels, which has been subject to great attention. In this paper we consider a fluid-structure interaction problem involving a two-dimensional viscoelastic fluid and a one-dimensional generalized rod structure. Until now, most of the existing papers concerning a fluid-structure system describe the blood as a Newtonian fluid [4, 10]. However, strictly speaking, blood is non-Newtonian due to it's complex nature. In fact, several investigations [22, 18, 14, 2, 3] have shown that the non-Newtonian characteristics of blood impact the characteristics of blood flow significantly. Motivated by the results, this work considers computational algorithms to examine the behavior of viscoelastic fluids in a moving domain or in a deformable elastic structure.

First, we consider a fluid defined on a domain which changes in time, where a boundary movement is specified by a known function. Several techniques have been proposed in the literature to simulate the *moving domain* problem. These approaches include level set method [6], Arbitrary Lagrangian Eulerian (ALE) formulation [4, 10], space time approach [29, 21] and immersed boundary method [4, 10]. Among these approaches, the ALE method, which was developed in the 1980's to post a coupled problem in a single framework [8, 13], is well formulated in the setting of the finite element method, and this is what we consider in the thesis.

In [23], the ALE method was used by F.Nobile to simulate a Newtonian fluid-structure system consisting of Navier-Stokes equations and an elastic structure. In following years, several related problems such as using various boundary conditions [9, 12, 24] and numerical stability [7, 12] were investigated. Also in [20], Martin et al. proved a convergence result of the ALE method for

the Stokes equations in a domain depending on time.

In [19], a quasi-Newtonian model in a moving domain was investigated by H.Lee. Given a boundary velocity by a known function, a numerical approximation of the unsteady flow problem was shown. In that paper, the ALE method was employed to derive the corresponding variational formulation. A priori error estimates for the semi-discrete and fully discrete ALE formulations, respectively, were obtained as well as stability and accuracy. Several numerical tests that match the theoretical results have also been presented.

Generally speaking, the ALE method is based on defining a mapping from a fixed reference domain to a physical, moving domain. This mapping actually introduces a relationship between a ALE coordinate and a physical coordinate. Since we can easily define a triangulation on the fixed reference domain, triangulations on current time can be easily obtained as the image of reference triangulation. With that mapping, we must work with a time derivative term on the ALE frame.

This thesis is organized as follows. In Chapter 2, we discuss approximations of a viscoelastic fluid on a moving domain. In this section, the boundary is defined by a given function. We derive the ALE formulation of the fluid and consider the finite element approximations of the problem. Both space discretization and time discretization schemes are discussed. Then, we present numerical results for this moving domain problem.

We consider a viscoelastic fluid-structure interaction problem in Chapter 3. Differing from the problem considered in Chapter 2, the boundary of the fluid is defined by the deformation of the wall rather than by a known function. A decoupling time discretization scheme is discussed and we present the numerical results for the fluid-system problem. Finally, in Chapter 4, we present the conclusion and future works.

Chapter 2

Viscoelastic flows in a moving domain

2.1 Notation and Model Equations

In this chapter, we will consider a two-dimensional Johnson-Segalman viscoelastic fluid defined on a moving domain. At any time t, Ω_t denotes the current domain for the fluid in $\mathbb{R}^2$. The Lipschitz continuous Γ_t is the corresponding moving boundary, while Γ_{tin} and Γ_{tout} are the inflow and outflow sides, respectively. A time-dependent boundary position function, $\mathbf{h}_t : \Gamma_0 \times [0,T] \to \Gamma_t$ such that $\Gamma_t = \mathbf{h}_t(t, \Gamma_0)$, will be given to describe the movement of Γ_t.

Consider the viscoelastic model equations:

$$\boldsymbol{\sigma} + \lambda \left(\frac{\partial \boldsymbol{\sigma}}{\partial t} + \mathbf{u} \cdot \nabla \boldsymbol{\sigma} + g_a(\boldsymbol{\sigma}, \nabla \mathbf{u}) \right) - 2\,\alpha\, D(\mathbf{u}) = \mathbf{0} \quad \text{in } \Omega_t\,, \tag{2.1}$$

$$\rho \left(\frac{\partial \mathbf{u}}{\partial t} + \mathbf{u} \cdot \nabla \mathbf{u} \right) - \nabla \cdot \boldsymbol{\sigma} - 2(1-\alpha)\, \nabla \cdot D(\mathbf{u}) + \nabla p = \mathbf{f} \quad \text{in } \Omega_t\,, \tag{2.2}$$

$$\nabla \cdot \mathbf{u} = 0 \quad \text{in } \Omega_t\,, \tag{2.3}$$

in (2.1) and (2.2), $D(\mathbf{u}) := \frac{(\nabla \mathbf{u} + \nabla \mathbf{u}^T)}{2}$ is a symmetric term called the rate of strain tensor. In (2.1),

$g_a(\boldsymbol{\sigma}, \nabla \mathbf{u})$ is defined as

$$g_a(\boldsymbol{\sigma}, \nabla \mathbf{u}) := \frac{1-a}{2}(\boldsymbol{\sigma}\nabla \mathbf{u} + \nabla \mathbf{u}^T \boldsymbol{\sigma}) - \frac{1+a}{2}(\nabla \mathbf{u}\, \boldsymbol{\sigma} + \boldsymbol{\sigma}\nabla \mathbf{u}^T), \qquad a \in [-1, 1]. \tag{2.4}$$

In (2.1)-(2.3), $\mathbf{u}$, $\boldsymbol{\sigma}$ and p denote the unknown velocity vector, polymeric stress tensor and pressure of the fluid, respectively. To specify the pressure p, we assume that p has mean value zero over the domain Ω_t. The Weissenberg number, λ, is the product of the relaxation time and a characteristic strain rate. The parameter ρ represents the density of the fluid and $\alpha \in (0, 1)$ can be considered as the fraction of viscoelastic viscosity. The right hand side function $\mathbf{f}$ in (2.2) is the body force exerted on the fluid. Also, notice that for a special case $a = 1$, (2.1) reduces to the Oldroyd-B model.

The initial values for the velocity and stress in Ω_0 are given as $\mathbf{u}^0$ and $\boldsymbol{\sigma}^0$, respectively. The boundary conditions are given as

$$\mathbf{u} = \mathbf{u}_{BC} \quad \text{on } \Gamma_t\,, \tag{2.5}$$

$$\boldsymbol{\sigma} = \boldsymbol{\sigma}_{BC} \quad \text{on } \Gamma_{tin}, \tag{2.6}$$

where $\int_{\Gamma_t} \mathbf{u}_{BC} \cdot \mathbf{n}\, d\Gamma_t = 0$.

2.2 The Arbitrary Lagrangian Eulerian (ALE) Formulation

In most fluid-structure interaction problems, fluid equations and structure equations are posed from different perspectives in continuum mechanics: the Eulerian frame of reference is used for the fluid equations, and the Lagrangian frame of reference for elastic structures. The ALE [8] method allows the coupled problem to be posed in one framework, and therefore is widely used in simulating fluid flows in a moving domain.

Generally speaking, the first step of ALE is to introduce a family of time-dependent mappings from a fixed reference domain to the physical moving domain. In this work, let the initial domain configuration Ω_0 be the reference domain. Then for any time $t \in (0, T]$, we can define a

mapping Ψ_t which maps a point in the reference domain Ω_0 to a point in the physical domain Ω_t:

$$\Psi_t : \Omega_0 \to \Omega_t, \qquad \Psi_t(\mathbf{Y}) = \mathbf{x}(\mathbf{X}, t)\,, \tag{2.7}$$

where $\mathbf{Y}$ is the ALE coordinate in Ω_0 and $\mathbf{x}$ is the spatial coordinate in Ω_t. In addition, we assume that Ψ_t is invertible and Ψ_t^{-1} is continuous.

The ALE mapping introduces a one-to-one coordinate transformation for the domain, so the fluid equations can be rewritten with respect to a fixed domain. It follows that at each time step, after determining the transformation function Ψ_t, the problem turns into a numerical simulation for a fluid defined on a fixed domain, which we are familiar with.

For any function $\phi : \Omega_t \times [0, T] \to \mathbb{R}$ posed on the Eulerian frame, we may define its corresponding function $\overline{\phi} = \phi \circ \Psi_t$ on the ALE frame as

$$\overline{\phi} : \Omega_0 \to \mathbb{R}, \qquad \overline{\phi}(\mathbf{Y}, t) = \phi(\Psi_t(\mathbf{Y}), t). \tag{2.8}$$

At the same time, its corresponding time derivative on the ALE frame is defined as

$$\frac{\partial \phi}{\partial t}\,|_{\mathbf{Y}} \colon \Omega_t \times [0, T] \to \mathbb{R}, \qquad \frac{\partial \phi}{\partial t}\,|_{\mathbf{Y}}\,(\mathbf{x}, t) = \frac{\partial \overline{\phi}}{\partial t}(\mathbf{Y}, t). \tag{2.9}$$

Using the above notation, the domain velocity can then be defined as $\mathbf{z} := \frac{\partial \mathbf{x}}{\partial t}\,|_{\mathbf{y}}$, which is actually the time derivative of Eulerian coordinate. Notice that $\mathbf{z}$ gives the velocity of each mesh node when discretized, so it is also called the mesh velocity.

Applying the chain rule, the ALE derivative of ϕ can be computed as

$$\frac{\partial \phi}{\partial t}\,|_{\mathbf{y}} = \frac{\partial \phi}{\partial t}\,|_{\mathbf{x}} + \mathbf{z} \cdot \nabla_{\mathbf{x}} \phi, \tag{2.10}$$

hence we can replace the time derivative term on the Eulerian frame by the ALE derivative

$$\frac{\partial \phi}{\partial t}\,|_{\mathbf{x}} = \frac{\partial \phi}{\partial t}\,|_{\mathbf{y}} - \mathbf{z} \cdot \nabla_{\mathbf{x}} \phi. \tag{2.11}$$

Then, the ALE formulation for the flow equations (2.1)-(2.3) obtained is

$$\boldsymbol{\sigma} + \lambda \left(\frac{\partial \boldsymbol{\sigma}}{\partial t} \mid_{\mathbf{y}} + (\mathbf{u} - \mathbf{z}) \cdot \nabla_{\mathbf{x}} \boldsymbol{\sigma} + g_a(\boldsymbol{\sigma}, \nabla_{\mathbf{x}} \mathbf{u}) \right) - 2\,\alpha\, D_{\mathbf{x}}(\mathbf{u}) = \mathbf{0} \quad \text{in } \Omega_t\,, \tag{2.12}$$

$$\rho \left(\frac{\partial \mathbf{u}}{\partial t} \mid_{\mathbf{y}} + (\mathbf{u} - \mathbf{z}) \cdot \nabla_{\mathbf{x}} \mathbf{u} \right) - \nabla_{\mathbf{x}} \cdot \boldsymbol{\sigma} - 2(1-\alpha)\, \nabla_{\mathbf{x}} \cdot D_{\mathbf{x}}(\mathbf{u}) + \nabla_{\mathbf{x}} p = \mathbf{f} \quad \text{in } \Omega_t\,, \tag{2.13}$$

$$\nabla_{\mathbf{x}} \cdot \mathbf{u} = 0 \quad \text{in } \Omega_t\,, \tag{2.14}$$

where $D_{\mathbf{x}}(\mathbf{u}) = (\nabla_{\mathbf{x}} \mathbf{u} + \nabla_{\mathbf{x}} \mathbf{u}^T)/2$.

The time derivative terms in (2.12)-(2.14) are now represented on the ALE frame, which are allowed to be computed along a constant $\mathbf{Y}$ line. On the other hand, all space derivative terms, including the divergence operator, are left expressed with respect to the Eulerian coordinate $\mathbf{x}$, which have simpler expression. To simplify notation, if not specified, $D(\cdot)$, ∇ refers to $D_{\mathbf{x}}(\cdot)$, $\nabla_{\mathbf{x}}$, respectively, throughout this thesis.

2.3 ALE Mapping Defining

One way to define the ALE mapping Ψ_t is the *harmonic extension technique* [10]. This name comes from the fact that we extend the boundary position function $\mathbf{h}_t : \Gamma_0 \times [0,T] \to \Gamma_t$ into the whole domain. This is a simple alternative to other techniques where we need to know the ALE mapping only at the discrete time level. That is, given the reference domain Ω_0 and the boundary position function $\mathbf{h}_t$, we solve the Laplace equation

$$\begin{cases} \Delta_{\mathbf{Y}} \Psi_t(\mathbf{Y}) = 0 & \text{in } \Omega_0\,, \\ \Psi_t(\mathbf{Y}) = \mathbf{h}_t(\mathbf{Y}) & \text{on } \Gamma_0\,. \end{cases}$$

Other equations such as a parabolic system can also be used to compute the domain velocity [10] in some problems.

2.4 Finite Element Discretization

2.4.1 Weak Formulation

The function spaces for the fixed reference domain Ω_0 are defined as:

$$\begin{cases} \mathbf{U}_0 := \mathbf{H}^1(\Omega_0)\,, \\ \overline{\mathbf{U}}_0 := \mathbf{H}^1_0(\Omega_0)\,, \\ Q_0 := L^2_0(\Omega_0) = \{\overline{q} \in L^2(\Omega_0) : \int_{\Omega_0} \overline{q}\, d\Omega = 0\}\,, \\ \boldsymbol{\Sigma}_0 := \{\boldsymbol{\tau} \in \mathbf{L}^2(\Omega_0) : \tau_{ij} = \tau_{ji},\}, \\ \overline{\boldsymbol{\Sigma}}_0 := \{\boldsymbol{\tau} \in \mathbf{L}^2(\Omega_0) : \tau_{ij} = \tau_{ji},\ \boldsymbol{\tau} = \mathbf{0} \text{ on } \Gamma_{tin}\}\,. \end{cases}$$

By the assumption we made before, the ALE mapping is invertible. Hence, the function spaces for the physical domain Ω_t can be derived from above function spaces as:

$$\begin{cases} \mathbf{U}_t := \{\mathbf{v} : \Omega_t \times [0,T] \to \mathbb{R}^2,\ \mathbf{v} = \overline{\mathbf{v}} \circ \Psi_t^{-1} \text{ for } \overline{\mathbf{v}} \in \mathbf{U}_0\}\,, \\ Q_t := \{q : \Omega_t \times [0,T] \to \mathbb{R},\ q = \overline{q} \circ \Psi_t^{-1} \text{ for } \overline{p} \in Q_0\}\,, \\ \overline{\mathbf{U}}_t := \{\mathbf{v} : \Omega_t \times [0,T] \to \mathbb{R}^2,\ \mathbf{v} = \overline{\mathbf{v}} \circ \Psi_t^{-1} \text{ for } \overline{\mathbf{v}} \in \overline{\mathbf{U}}_0\}\,, \\ \boldsymbol{\Sigma}_t := \{\boldsymbol{\tau} : \Omega_t \times [0,T] \to \mathbb{R}^{2\times 2},\ \boldsymbol{\tau} = \overline{\boldsymbol{\tau}} \circ \Psi_t^{-1} \text{ for } \overline{\boldsymbol{\tau}} \in \boldsymbol{\Sigma}_0\}, \\ \overline{\boldsymbol{\Sigma}}_t := \{\boldsymbol{\tau} : \Omega_t \times [0,T] \to \mathbb{R}^{2\times 2},\ \boldsymbol{\tau} = \overline{\boldsymbol{\tau}} \circ \Psi_t^{-1} \text{ for } \overline{\boldsymbol{\tau}} \in \overline{\boldsymbol{\Sigma}}_0\}\,. \end{cases}$$

In fact,

$$(\mathbf{v}, q, \boldsymbol{\tau}) \in \mathbf{U}_t \times Q_t \times \boldsymbol{\Sigma}_t \text{ if and only if } (\overline{\mathbf{v}}, \overline{q}, \overline{\boldsymbol{\tau}}) = (\mathbf{v} \circ \Psi_t, q \circ \Psi_t, \boldsymbol{\tau} \circ \Psi_t) \in \mathbf{U}_0 \times Q_0 \times \boldsymbol{\Sigma}_0\,, \quad (2.15)$$

provided the ALE mapping Ψ_t is invertible and has sufficient regularity [10, 20]. The weak formulation in the ALE framework is given by:

find $(\mathbf{u}, p, \boldsymbol{\sigma}) \in \mathbf{U}_t \times Q_t \times \boldsymbol{\Sigma}_t$ such that

$$(\boldsymbol{\sigma},\, \boldsymbol{\tau})_{\Omega_t} + \lambda \left(\frac{\partial \boldsymbol{\sigma}}{\partial t} \mid_{\mathbf{y}} + ((\mathbf{u}-\mathbf{z})\cdot\nabla)\boldsymbol{\sigma} + g_a(\boldsymbol{\sigma}, \nabla\mathbf{u}),\, \boldsymbol{\tau} \right)_{\Omega_t}$$
$$-2\alpha\,(D(\mathbf{u}),\, \boldsymbol{\tau})_{\Omega_t} = \mathbf{0}, \qquad \forall \boldsymbol{\tau} \in \overline{\boldsymbol{\Sigma}}_t\,, \quad (2.16)$$

$$\rho \left(\frac{\partial \mathbf{u}}{\partial t} \mid_{\mathbf{y}} + (\mathbf{u}-\mathbf{z})\cdot\nabla\mathbf{u},\, \mathbf{v} \right)_{\Omega_t} + (\boldsymbol{\sigma}, D(\mathbf{v}))_{\Omega_t}$$
$$+2(1-\alpha)(D(\mathbf{u}), D(\mathbf{v}))_{\Omega_t} - (p, \nabla\cdot\mathbf{v})_{\Omega_t} = (\mathbf{f}, \mathbf{v})_{\Omega_t}\,, \qquad \forall \mathbf{v} \in \overline{\mathbf{U}}_t\,, \quad (2.17)$$

$$(q, \nabla\cdot\mathbf{u})_{\Omega_t} = 0, \qquad \forall q \in Q_t\,. \quad (2.18)$$

Similarly, as shown for the quasi-Newtonian case in [19], using the Reynolds transportation formula

$$\frac{d}{dt}\int_{V(t)} \phi(\mathbf{x}, t)\, dV = \int_{V(t)} \frac{\partial \phi}{\partial t} \mid_{\mathbf{y}} + \phi \nabla_{\mathbf{x}}\cdot\mathbf{z}\, dV = \int_{V(t)} \frac{\partial \phi}{\partial t} \mid_{\mathbf{x}} + \mathbf{z}\cdot\nabla_{\mathbf{x}}\phi + \phi\nabla_{\mathbf{x}}\cdot\mathbf{z}\, dV, \quad (2.19)$$

we have for a function $\phi : V(t) \to \mathbb{R}$, where $V(t) = \Psi_t(V_0) \subset \Omega_t$, $V_0 \subset \Omega_0$ [25],

$$\left(\frac{\partial \phi}{\partial t} \mid_{\mathbf{y}}, v \right) = \frac{d}{dt}\,(\phi, v) - (\phi\nabla_{\mathbf{x}}\cdot\mathbf{z}, v)\,. \quad (2.20)$$

Applying (2.20) to (2.16)-(2.18), we can obtain a variational formulation of the fluid as: for each $t \in (0, T]$, find $(\mathbf{u}, p, \boldsymbol{\sigma}) \in \mathbf{U}_t \times Q_t \times \boldsymbol{\Sigma}_t$ such that

$$(\boldsymbol{\sigma}, \boldsymbol{\tau})_{\Omega_t} + \lambda \frac{d}{dt}(\boldsymbol{\sigma}, \boldsymbol{\tau})_{\Omega_t} + \lambda\,(-\boldsymbol{\sigma}(\nabla\cdot\mathbf{z}) + ((\mathbf{u}-\mathbf{z})\cdot\nabla)\boldsymbol{\sigma} + g_a(\boldsymbol{\sigma}, \nabla\mathbf{u}),\, \boldsymbol{\tau})_{\Omega_t}$$
$$-2\alpha(D(\mathbf{u}), \boldsymbol{\tau})_{\Omega_t} = \mathbf{0}, \qquad \forall \boldsymbol{\tau} \in \overline{\boldsymbol{\Sigma}}_t\,, \quad (2.21)$$

$$\rho \frac{d}{dt}(\mathbf{u}, \mathbf{v})_{\Omega_t} + \rho\,(-\mathbf{u}(\nabla\cdot\mathbf{z}) + ((\mathbf{u}-\mathbf{z})\cdot\nabla)\mathbf{u},\, \mathbf{v})_{\Omega_t}$$
$$+2(1-\alpha)(D(\mathbf{u}),\, D(\mathbf{v}))_{\Omega_t} + (\boldsymbol{\sigma}, D(\mathbf{v}))_{\Omega_t} - (p, \nabla\cdot\mathbf{v})_{\Omega_t} = (\mathbf{f}, \mathbf{v})_{\Omega_t}\,, \qquad \forall \mathbf{v} \in \overline{\mathbf{U}}_t \quad (2.22)$$

$$(q, \nabla\cdot\mathbf{u})_{\Omega_t} = 0, \qquad \forall q \in Q_t\,. \quad (2.23)$$

2.4.2 Finite Element Discretization

In order to find a numerical solution for the moving domain problem, in general we need to find (i)the ALE mapping and (ii)a weak solution of the fluid equation.

For spatial discretization, suppose Ω_0 is discretized by a triangulation $T_{h,0}$ with a maximum diameter h. Assume the discretized domain $\overline{\Omega}_0 := \{\cup K : K \in T_{h,0}\} = \Omega_0$. Let $P_k(K)$ denote the space of polynomials of degree k on $K \in T_{h,0}$. For $(\mathbf{u}, p)$, we use the the Taylor-Hood pair (P_2, P_1), which are known to satisfy the LBB condition:

$$\inf_{0 \neq q_h \in Q_{h,0}} \sup_{0 \neq \mathbf{v}_h \in \mathbf{U}_{h,0}} \frac{(q_h, \nabla \cdot \mathbf{v}_h)}{\|\mathbf{v}_h\|_1 \|q_h\|_0} \geq C\,, \tag{2.24}$$

where C is a positive constant independent of h. Thus, the finite element spaces for $(\mathbf{u}, p)$ in Ω_0 are defined as:

$$\begin{aligned}
\mathbf{U}_{h,0} &:= \{\mathbf{v} \in \mathbf{U}_0 \cap (C^0(\overline{\Omega}))^2 : \mathbf{v}|_K \in P_2(K)^2,\ \forall K \in T_{h,0}\}\,, \\
\overline{\mathbf{U}}_{h,0} &:= \{\mathbf{v} \in \mathbf{U}_{h,0} : \mathbf{v} = 0 \quad on \quad \Gamma_0\}, \\
Q_{h,0} &:= \{q \in Q_0 \cap C^0(\overline{\Omega}) : q|_K \in P_1(K),\ \forall K \in T_{h,0}\}\,.
\end{aligned}$$

For the stress $\boldsymbol{\sigma}$, we use the discontinuous piecewise linear finite element space as follows:

$$\begin{aligned}
\boldsymbol{\Sigma}_{h,0} &:= \{\boldsymbol{\tau} \in \boldsymbol{\Sigma}_0 : \boldsymbol{\tau}|_K \in P_1(K)^{2\times 2},\ \forall K \in T_{h,0}\}\,, \\
\overline{\boldsymbol{\Sigma}}_{h,0} &:= \{\boldsymbol{\tau} \in \boldsymbol{\Sigma}_{h,0} : \boldsymbol{\tau} = 0 \quad on \quad \Gamma_{0in}\}.
\end{aligned}$$

If we use P_1 Lagrangian finite elements

$$\mathbf{X}_h := \{\mathbf{x} \in \mathbf{H}^1(\Omega_0) : \mathbf{x}|_K \in P_1(K)^2,\ \forall K \in T_{h,0}\} \tag{2.25}$$

to find a discrete ALE mapping, $\Psi_{h,t} : \Omega_0 \to \Omega_t$ such that $\Psi_{h,t}(y) = \mathbf{x}_h(\mathbf{y}, t)$, then for each time t, the corresponding finite element spaces for Ω_t are defined as:

$$\begin{aligned}
\mathbf{U}_{h,t} &:= \{\mathbf{v}_h : \Omega_t \times [0,T] \to \mathbb{R}^2, \mathbf{v}_h = \overline{\mathbf{v}}_h \circ \Psi_{h,t}^{-1} \text{ for } \overline{\mathbf{v}}_h \in \mathbf{U}_{h,0}\}\,, \\
\overline{\mathbf{U}}_{h,t} &:= \{\mathbf{v}_h : \Omega_t \times [0,T] \to \mathbb{R}^2, \mathbf{v}_h = \overline{\mathbf{v}}_h \circ \Psi_{h,t}^{-1} \text{ for } \overline{\mathbf{v}}_h \in \overline{\mathbf{U}}_{h,0}\}\,, \\
Q_{h,t} &:= \{q_h : \Omega_t \times [0,T] \to \mathbb{R}, q_h = \overline{q}_h \circ \Psi_{h,t}^{-1} \text{ for } \overline{q}_h \in Q_{h,0}\}\,, \\
\boldsymbol{\Sigma}_{h,t} &:= \{\boldsymbol{\sigma}_h : \Omega_t \times [0,T] \to \mathbb{R}^{2\times 2}, \boldsymbol{\sigma}_h = \overline{\boldsymbol{\sigma}}_h \circ \Psi_t^{-1} \text{ for } \overline{\boldsymbol{\sigma}}_h \in \boldsymbol{\Sigma}_{h,0}\}, \\
\overline{\boldsymbol{\Sigma}}_{h,t} &:= \{\boldsymbol{\sigma}_h : \Omega_t \times [0,T] \to \mathbb{R}^{2\times 2}, \boldsymbol{\sigma}_h = \overline{\boldsymbol{\sigma}}_h \circ \Psi_t^{-1} \text{ for } \overline{\boldsymbol{\sigma}}_h \in \overline{\boldsymbol{\Sigma}}_{h,0}\}.
\end{aligned}$$

Let $\{\overline{\varphi}_i : \overline{\varphi}_i \in \mathbf{U}_{h,0}\}$ and $\{\overline{\psi}_i : \overline{\psi}_i \in \mathbf{\Sigma}_{h,0}\}$ be sets of basis functions for $\mathbf{U}_{h,0}$ and $\mathbf{\Sigma}_{h,0}$, respectively. Then, the approximations for velocity and stress can be represented as linear combinations of basis functions, respectively, i.e.,

$$\mathbf{u}_h(\mathbf{x},t) = \sum_{i\in\mathcal{N}_{\tilde{u}}} u_i(t)\varphi_i(\mathbf{x},t)\,, \qquad \boldsymbol{\sigma}_h(\mathbf{x},t) = \sum_{i\in\mathcal{N}_{\sigma}} \sigma_i(t)\psi_i(\mathbf{x},t)\,, \tag{2.26}$$

where $\varphi_i := \overline{\varphi}_i \circ \Psi_t^{-1}$ and $\psi_i := \overline{\psi}_i \circ \Psi_t^{-1}$.

To approximate the stress $\boldsymbol{\sigma}$, we introduce the following notation to apply the discontinuous Galerkin method:

$$\partial K^-(\mathbf{v}) := \{\mathbf{x} \in \partial K,\ \mathbf{v}\cdot\mathbf{n} < 0\}\,,$$

where ∂K is the boundary of K and $\mathbf{n}$ is the outward unit normal to ∂K,

$$\boldsymbol{\tau}^{\pm}(\mathbf{v}) := \lim_{\epsilon\to 0^{\pm}} \boldsymbol{\tau}(\mathbf{x}+\epsilon\mathbf{v}(\mathbf{x}))\,.$$

With the above notation,

$$< \boldsymbol{\sigma}^{\pm}, \boldsymbol{\tau}^{\pm} >_{h,\mathbf{v}} := \sum_{K\in T_{h,t}} \int_{\partial K^-(\mathbf{v})} (\boldsymbol{\sigma}^{\pm} : \boldsymbol{\tau}^{\pm})|\mathbf{n}\cdot\mathbf{v}|\ ds\,.$$

We also define the operator $c(\cdot,\cdot,\cdot)$ by

$$c(\mathbf{v}-\mathbf{z},\boldsymbol{\sigma},\boldsymbol{\tau})_{\Omega_t} := (((\mathbf{v}-\mathbf{z})\cdot\nabla)\boldsymbol{\sigma},\boldsymbol{\tau})_{\Omega_t} + < \boldsymbol{\sigma}^+ - \boldsymbol{\sigma}^-, \boldsymbol{\tau}^+ >_{h,\mathbf{v}-\mathbf{z}} \tag{2.27}$$

to simplify our expressions.

The semi-discrete variational formulation of the fluid problem (2.1)-(2.3) in the ALE framework can be written as:

find $(\mathbf{u}_h, p_h, \boldsymbol{\sigma}_h) \in \mathbf{U}_t \times Q_t \times \boldsymbol{\Sigma}_t$ such that

$$\lambda \left[\frac{d}{dt}(\boldsymbol{\sigma}_h, \boldsymbol{\tau}_h)_{\Omega_t} + c(\mathbf{u}_h - \mathbf{z}_h, \boldsymbol{\sigma}_h, \boldsymbol{\tau}_h)_{\Omega_t} - (\boldsymbol{\sigma}_h(\nabla \cdot \mathbf{z}_h), \boldsymbol{\tau}_h)_{\Omega_t} \right.$$
$$\left. + (g_a(\boldsymbol{\sigma}_h, \nabla \mathbf{u}),\, \boldsymbol{\tau}_h)_{\Omega_t} \right] + (\boldsymbol{\sigma}_h, \boldsymbol{\tau}_h)_{\Omega_t}$$
$$- 2\alpha(D(\mathbf{u}_h), \boldsymbol{\tau}_h)_{\Omega_t} = \mathbf{0} \qquad \forall \boldsymbol{\tau}_h \in \overline{\boldsymbol{\Sigma}}_{h,t}\,, \quad (2.28)$$

$$\rho \left[\frac{d}{dt}(\mathbf{u}_h, \mathbf{v}_h)_{\Omega_t} + (\mathbf{u}_h \cdot \nabla \mathbf{u}_h, \mathbf{v}_h)_{\Omega_t} - (\mathbf{u}_h(\nabla \cdot \mathbf{z}_h), \mathbf{v}_h)_{\Omega_t} - (\mathbf{z}_h \cdot \nabla u_h, \mathbf{v}_h)_{\Omega_t} \right]$$
$$+ 2(1-\alpha)(D(\mathbf{u}_h),\, D(\mathbf{v}_h))_{\Omega_t} + (\boldsymbol{\sigma}_h, D(\mathbf{v}_h))_{\Omega_t} + (p_h, \nabla \cdot \mathbf{v}_h)_{\Omega_t}$$
$$= (\mathbf{f}, \mathbf{v}_h)_{\Omega_t} \qquad \forall \mathbf{v}_h \in \overline{\mathbf{U}}_{h,t}\,, \quad (2.29)$$

$$(q_h, \nabla \cdot \mathbf{u}_h)_{\Omega_t} = 0 \qquad \forall q_h \in Q_{h,t}\,. \quad (2.30)$$

2.4.3 Geometric conservation law

In moving domain problems, the Geometric conservation law (GCL), which is known to be related to the stability of the numerical approximation, is a popular tool which has been used to develop a finite volume scheme while preserving the volume of a cell. It states that for each time step interval (t_n, t_{n+1}), a quadrature rule should be chosen appropriately such that the identity

$$\int_{\Omega_{t^{n+1}}} \mathbf{v}_h \, d\Omega - \int_{\Omega_{t^n}} \mathbf{v}_h \, d\Omega = \int_{t^n}^{t^{n+1}} \int_{\Omega_t} \mathbf{v}_h \nabla \cdot \mathbf{z}_h \, d\Omega \, dt \quad (2.31)$$

is performed exactly.

Suppose that d is the space dimension, and k is the degree of the piecewise polynomial used for the ALE mapping. It has been reported that an integration formula of degree $k \times d - 1$ or more should be used to guarantee the GCL [28], i.e. a quadrature rule should be exact for the integration

$$\int_{\Omega_{t^{n+1}}} \mathbf{v}_h \, d\Omega - \int_{\Omega_{t^n}} \mathbf{v}_h \, d\Omega \approx \int_{t^n}^{t^{n+1}} \mathbf{p}(s) \, ds,$$

where $\mathbf{p}(t)$ is a polynomial for $t \in [t^n, t^{n+1}]$ of degree $k \times d - 1$. For instance, in a two-dimensional problem where piecewise linear elements are used for are ALE mapping, the degree of precision of the quadrature rule should be at least 1. Hence, both the mid-point and trapezoidal rule satisfy GCL.

2.4.4 Two time Discretization methods

For temporal discretization of the problem (2.28)-(2.30), we consider two methods: the implicit Euler method and Crank-Nicolson method. In the following, $\mathbf{u}^n$ is used as a simplified notation of $\mathbf{u}_h^n$, which is an approximate of $\mathbf{u}_h(t^n)$.

First, we discretize the problem by the standard implicit Euler scheme:

$$\begin{aligned}
&\lambda\left[(\boldsymbol{\sigma}^{n+1},\boldsymbol{\tau})_{\Omega_{t^{n+1}}}-(\boldsymbol{\sigma}^{n},\boldsymbol{\tau})_{\Omega_{t^{n}}}\right]+\lambda\,\Delta t\left[c(\mathbf{u}^{n+1}-\mathbf{z}^{n+1},\boldsymbol{\sigma}^{n+1},\boldsymbol{\tau})_{\Omega_{t^{n+1}}}\right.\\
&\quad\left.-(\boldsymbol{\sigma}^{n+1}(\nabla\cdot\mathbf{z}^{n+1}),\boldsymbol{\tau})_{\Omega_{t^{n+1}}}+(g_a(\boldsymbol{\sigma}^{n+1},\nabla\mathbf{u}^{n+1}),\,\boldsymbol{\tau})_{\Omega_{t^{n+1}}}\right]\\
&\quad+\Delta t\left[(\boldsymbol{\sigma}^{n+1},\boldsymbol{\tau})_{\Omega_{t^{n+1}}}-2\alpha(D(\mathbf{u}^{n+1}),\boldsymbol{\tau})_{\Omega_{t^{n+1}}}\right]=\mathbf{0}\,, \qquad \forall\boldsymbol{\tau}\in\overline{\boldsymbol{\Sigma}}_{h,t}\,, \quad (2.32)
\end{aligned}$$

$$\begin{aligned}
&\rho\left[(\mathbf{u}^{n+1},\mathbf{v})_{\Omega_{t^{n+1}}}-(\mathbf{u}^{n},\mathbf{v})_{\Omega_{t^{n}}}\right]+\Delta t\,\rho\left[\,(\mathbf{u}^{n+1}\cdot\nabla\mathbf{u}^{n+1},\mathbf{v})_{\Omega_{t^{n+1}}}\right.\\
&\quad\left.-(\mathbf{u}^{n+1}(\nabla\cdot\mathbf{z}^{n+1}),\mathbf{v})_{\Omega_{t^{n+1}}}-(\mathbf{z}^{n+1}\cdot\nabla\mathbf{u}^{n+1},\mathbf{v})_{\Omega_{t^{n+1}}}\right]\\
&\quad+\Delta t\left[2(1-\alpha)(D(\mathbf{u}^{n+1}),\,D(\mathbf{v}))_{\Omega_{t^{n+1}}}+(\boldsymbol{\sigma}^{n+1},D(\mathbf{v}))_{\Omega_{t^{n+1}}}+(p^{n+1},\nabla\cdot\mathbf{v})_{\Omega_{t^{n+1}}}\right]\\
&=\Delta t(\mathbf{f}^{n+1},\mathbf{v})_{\Omega_{t^{n+1}}}\,, \qquad \forall\mathbf{v}\in\overline{\mathbf{U}}_{h,t}\,, \quad (2.33)
\end{aligned}$$

$$(q,\nabla\cdot\mathbf{u}^{n+1})_{\Omega_{t^{n+1}}}=0, \qquad \forall q\in Q_{h,t}\,. \quad (2.34)$$

However, the above equations do not satisfy the GCL. Applying the mid-point rule,

$$\int_{\Omega_{t^{n+1}}}\mathbf{v}_h\,d\Omega-\int_{\Omega_{t^n}}\mathbf{v}_h\,d\Omega=\int_{t^n}^{t^{n+1}}\int_{\Omega_t}\mathbf{v}_h\nabla\cdot\mathbf{z}_h\,d\Omega\,dt\approx\Delta t\int_{\Omega_{t^{n+\frac{1}{2}}}}\mathbf{v}_h\nabla\cdot\mathbf{z}_h\,ds, \qquad (2.35)$$

we have an implicit Euler scheme satisfying the GCL:

$$\begin{aligned}
&\lambda\left[(\boldsymbol{\sigma}^{n+1},\boldsymbol{\tau})_{\Omega_{t_{n+1}}}-(\boldsymbol{\sigma}^{n},\boldsymbol{\tau})_{\Omega_{t_n}}\right]+\lambda\,\Delta t\left[c(\mathbf{u}^{n+1}-\mathbf{z}^{n+\frac{1}{2}},\boldsymbol{\sigma}^{n+1},\boldsymbol{\tau})_{\Omega_{t^{n+\frac{1}{2}}}}\right.\\
&\qquad\left.-(\boldsymbol{\sigma}^{n+1}(\nabla\cdot\mathbf{z}^{n+\frac{1}{2}}),\boldsymbol{\tau})_{\Omega_{t^{n+\frac{1}{2}}}}+(g_a(\boldsymbol{\sigma}^{n+1},\nabla\mathbf{u}^{n+1}),\,\boldsymbol{\tau})_{\Omega_{t^{n+\frac{1}{2}}}}\right]\\
&\qquad+\Delta t\left[(\boldsymbol{\sigma}^{n+1},\boldsymbol{\tau})_{\Omega_{t^{n+\frac{1}{2}}}}-2\alpha(D(\mathbf{u}^{n+1}),\boldsymbol{\tau})_{\Omega_{t^{n+\frac{1}{2}}}}\right]=\mathbf{0}, \qquad \forall\boldsymbol{\tau}\in\overline{\boldsymbol{\Sigma}}_{h,t}\,, \qquad (2.36)
\end{aligned}$$

$$\begin{aligned}
&\rho\left[(\mathbf{u}^{n+1},\mathbf{v})_{\Omega_{t^{n+1}}}-(\mathbf{u}^{n},\mathbf{v})_{\Omega_{t_n}}\right]+\Delta t\,\rho\left[(\mathbf{u}^{n+1}\cdot\nabla\mathbf{u}^{n+1},\mathbf{v})_{\Omega_{t^{n+\frac{1}{2}}}}\right.\\
&\qquad\left.-(\mathbf{u}^{n+1}(\nabla\cdot\mathbf{z}^{n+\frac{1}{2}}),\mathbf{v})_{\Omega_{t^{n+\frac{1}{2}}}}-(\mathbf{z}^{n+\frac{1}{2}}\cdot\nabla\mathbf{u}^{n+1},\mathbf{v})_{\Omega_{t^{n+\frac{1}{2}}}}\right]\\
&\qquad+\Delta t\left[2(1-\alpha)(D(\mathbf{u}^{n+1}),\,D(\mathbf{v}))_{\Omega_{t^{n+\frac{1}{2}}}}+(\boldsymbol{\sigma}^{n+1},D(\mathbf{v}))_{\Omega_{t^{n+\frac{1}{2}}}}+(p^{n+1},\nabla\cdot\mathbf{v})_{\Omega_{t^{n+\frac{1}{2}}}}\right]\\
&=\Delta t(\mathbf{f}^{n+\frac{1}{2}},\mathbf{v})_{\Omega_{t^{n+\frac{1}{2}}}}\,, \qquad \forall\mathbf{v}\in\overline{\mathbf{U}}_{h,t}\,, \qquad (2.37)
\end{aligned}$$

$$(q,\nabla\cdot\mathbf{u}^{n+1})_{\Omega_{t^{n+\frac{1}{2}}}}=0, \qquad \forall q\in Q_{h,t}\,, \qquad (2.38)$$

where we note that most terms are computed in the half-time step domain $\Omega_{t^{n+\frac{1}{2}}}$, with the exception of the time derivative terms.

Similarly, the Crank-Nicolson scheme which satisfies the GCL reads as:

$$\lambda\left[(\boldsymbol{\sigma}^{n+1},\boldsymbol{\tau})_{\Omega_{t_{n+1}}}-(\boldsymbol{\sigma}^{n},\boldsymbol{\tau})_{\Omega_{t_n}}\right]+\lambda\,\Delta t\left[c\left(\frac{\mathbf{u}^{n+1}+\mathbf{u}^{n}}{2}-\mathbf{z}^{n+\frac{1}{2}},\frac{\boldsymbol{\sigma}^{n+1}+\boldsymbol{\sigma}^{n}}{2},\boldsymbol{\tau}\right)_{\Omega_{t^{n+\frac{1}{2}}}}\right.$$
$$\left.-\left(\frac{\boldsymbol{\sigma}^{n+1}+\boldsymbol{\sigma}^{n}}{2}(\nabla\cdot\mathbf{z}^{n+\frac{1}{2}}),\boldsymbol{\tau}\right)_{\Omega_{t^{n+\frac{1}{2}}}}+\left(g_a\left(\frac{\boldsymbol{\sigma}^{n+1}+\boldsymbol{\sigma}^{n}}{2},\nabla\frac{\mathbf{u}^{n+1}+\mathbf{u}^{n}}{2}\right),\boldsymbol{\tau}\right)_{\Omega_{t^{n+\frac{1}{2}}}}\right]$$
$$+\Delta t\left[\left(\frac{\boldsymbol{\sigma}^{n+1}+\boldsymbol{\sigma}^{n}}{2},\boldsymbol{\tau}\right)_{\Omega_{t^{n+\frac{1}{2}}}}-2\alpha\left(D\left(\frac{\mathbf{u}^{n+1}+\mathbf{u}^{n}}{2}\right),\boldsymbol{\tau}\right)_{\Omega_{t^{n+\frac{1}{2}}}}\right]=\mathbf{0}\quad\forall\boldsymbol{\tau}\in\overline{\boldsymbol{\Sigma}}_{h,t}\tag{2.39}$$

$$\rho\left[(\mathbf{u}^{n+1},\mathbf{v})_{\Omega_{t^{n+1}}}-(\mathbf{u}_h,\mathbf{v})_{\Omega_{t_n}}\right]+\Delta t\,\rho\left[\left(\frac{\mathbf{u}^{n+1}+\mathbf{u}^{n}}{2}\cdot\nabla\frac{\mathbf{u}^{n+1}+\mathbf{u}^{n}}{2},\mathbf{v}\right)_{\Omega_{t^{n+\frac{1}{2}}}}\right.$$
$$\left.-\left(\frac{\mathbf{u}^{n+1}+\mathbf{u}^{n}}{2}(\nabla\cdot\mathbf{z}^{n+\frac{1}{2}}),\mathbf{v}\right)_{\Omega_{t^{n+\frac{1}{2}}}}-\left(\mathbf{z}^{n+\frac{1}{2}}\cdot\nabla\frac{\mathbf{u}^{n+1}+\mathbf{u}^{n}}{2},\mathbf{v}\right)_{\Omega_{t^{n+\frac{1}{2}}}}\right]$$
$$+\Delta t\left[2(1-\alpha)\left(D\left(\frac{\mathbf{u}^{n+1}+\mathbf{u}^{n}}{2}\right),D(\mathbf{v})\right)_{\Omega_{t^{n+\frac{1}{2}}}}+\left(\frac{\boldsymbol{\sigma}^{n+1}+\boldsymbol{\sigma}^{n}}{2},D(\mathbf{v})\right)_{\Omega_{t^{n+\frac{1}{2}}}}\right.$$
$$\left.+(\frac{p^{n+1}+p^{n}}{2},\nabla\cdot\mathbf{v})_{\Omega_{t^{n+\frac{1}{2}}}}\right]=\Delta t(\mathbf{f}^{n+\frac{1}{2}},\mathbf{v})_{\Omega_{t^{n+\frac{1}{2}}}}\qquad\forall\mathbf{v}\in\overline{\mathbf{U}}_{h,t}\,,\tag{2.40}$$

$$\left(q,\nabla\cdot\frac{\mathbf{u}^{n+1}+\mathbf{u}^{n}}{2}\right)_{\Omega_{t^{n+\frac{1}{2}}}}=0\qquad\forall q\in Q_{h,t}\,.\tag{2.41}$$

2.5 Numerical results

In the previous section, we introduced two different time discretization methods. In this section, for the two methods, we present numerical results of two tests including calculated error rates. We test on the model equations:

$$\boldsymbol{\sigma}+\lambda\left(\frac{\partial\boldsymbol{\sigma}}{\partial t}+\mathbf{u}\cdot\nabla\boldsymbol{\sigma}+g_a(\boldsymbol{\sigma},\nabla\mathbf{u})\right)-2\,\alpha\,D(\mathbf{u})\;=\;\mathbf{f}_1,\quad\text{in }\Omega_t\,,\tag{2.42}$$

$$\rho\left(\frac{\partial\mathbf{u}}{\partial t}+\mathbf{u}\cdot\nabla\mathbf{u}\right)-\nabla\cdot\boldsymbol{\sigma}-2(1-\alpha)\,\nabla\cdot D(\mathbf{u})+\nabla p\;=\;\mathbf{f}_2,\quad\text{in }\Omega_t\,,\tag{2.43}$$

$$\nabla\cdot\mathbf{u}\;=\;0.\quad\text{in }\Omega_t\,.\tag{2.44}$$

A known function is given as the exact solution in order to test convergence rates of errors. At $t=0$, a rectangle $\Omega_0=\{\mathbf{y}:\mathbf{y}\in[0,1]\times[0,1]\}$ is chosen to be the initial domain. After that, for

any time $t \in (0, T]$, the time-dependent domain is defined as

$$\Omega_t = \{\mathbf{x} : x_1 = y_1\,(2 - \cos(\pi t)),\ x_2 = y_2\,(2 - \cos(\pi t)) \text{ for } \mathbf{y} \in \Omega_0\}. \tag{2.45}$$

Considering the moving domain defined above, we use the exact ALE mapping and the exact domain velocity given by

$$\mathbf{z} = \left[\frac{x_1 \pi \sin(\pi t)}{2 - \cos(\pi t)},\ \frac{x_2 \pi \sin(\pi t)}{2 - \cos(\pi t)}\right]^T. \tag{2.46}$$

The parameters in the model are chosen as $\lambda = 0.5$, $\alpha = 0.5$, $a = 0$, and the exact solution is given as

$$\begin{cases} \mathbf{u} = \begin{bmatrix} 10\sin(2\pi t + 1)x_1^2(x_1 - 1)^2 x_2(2x_2 - 1)(x_2 - 1) \\ -10\sin(2\pi t + 2)x_2^2(x_2 - 1)^2 x_1(2x_1 - 1)(x_1 - 1) \end{bmatrix} \\ p = \sin(\pi t + 2)\cos(2\pi x_1)x_2(x_2 - 1) \\ \boldsymbol{\sigma} = \begin{bmatrix} \sigma_{11} & \sigma_{12} \\ \sigma_{21} & \sigma_{22} \end{bmatrix} \end{cases}$$

in the initial domain, where

$$\begin{cases} \sigma_{11} = 10\sin(2\pi t + 1)x_1^2(x_1 - 1)^2 x_2(2x_2 - 1)(x_2 - 1) \\ \sigma_{12} = \sigma_{21} = -10\sin(2\pi t + 2)x_2^2(x_2 - 1)^2 x_1(2x_1 - 1)(x_1 - 1) \\ \sigma_{22} = 0. \end{cases}$$

With the above information, we can calculate right hand side functions $\mathbf{f}_1$, $\mathbf{f}_2$ so that the above exact solution satisfies the model equations.

In our numerical test for the fluid, the Taylor-Hood pair (P_2, P_1) is used for $(\mathbf{u}, p)$, while discontinuous piecewise linear elements are used to approximate the stress $\boldsymbol{\sigma}$.

In [1], Baranger and Sandri proved that the error bound of finite element approximation for a viscoelastic fluid flow in a fixed domain is

$$\|\boldsymbol{\sigma} - \boldsymbol{\sigma}_h\|_0 + \|D(\mathbf{u}) - D(\mathbf{u}_h)\|_0 \le C\,h^{3/2},$$

when $(P_2, P_1, P_{1\,DG})$ (Taylor-Hood, discontinuous linear) is used. However, it was observed that

$$\|\boldsymbol{\sigma} - \boldsymbol{\sigma}_h\|_0 + \|D(\mathbf{u}) - D(\mathbf{u}_h)\|_0 \leq C\,h^2,$$

in various numerical tests [16, 17] using the same finite elements.

Test one

In this test, with a fixed number of elements generated by 26×26 uniform grid initially, we computed the L^2, H^1 errors of velocity, and L^2 error of stress on various time steps $\Delta t = \frac{1}{2.5}, \frac{1}{5}, \frac{1}{10}, \frac{1}{15}, \frac{1}{20}, \frac{1}{30}$. With the number of elements chosen, we expected errors to be dominated by the time step when large Δt values are used. The results of implicit Euler and Crank-Nicolson methods are presented separately in Table 2.1 and Table 2.2.

	velocity				stress	
Δt	L^2 error	L^2 rate	H^1 error	H^1 rate	L^2 error	L^2 rate
$\frac{1}{2.5}$	$.1090 \cdot 10^{-2}$		$.4877 \cdot 10^{-2}$		$.1310 \cdot 10^{-2}$	
$\frac{1}{5}$	$.5140 \cdot 10^{-3}$	1.11	$.1974 \cdot 10^{-2}$	1.30	$.5539 \cdot 10^{-3}$	1.24
$\frac{1}{10}$	$.1820 \cdot 10^{-3}$	1.50	$.6523 \cdot 10^{-3}$	1.30	$.1683 \cdot 10^{-3}$	1.72
$\frac{1}{15}$	$.1019 \cdot 10^{-3}$	1.43	$.3801 \cdot 10^{-3}$	1.33	$.9393 \cdot 10^{-4}$	1.44
$\frac{1}{20}$	$.6905 \cdot 10^{-4}$	1.35	$.2673 \cdot 10^{-3}$	1.22	$.6404 \cdot 10^{-4}$	1.33
$\frac{1}{30}$	$.4114 \cdot 10^{-4}$	1.28	$.1670 \cdot 10^{-3}$	1.16	$.3822 \cdot 10^{-4}$	1.27

Table 2.1: Errors of velocity and stress by Implicit Euler for $t = 0.4$.

	velocity				stress	
Δt	L^2 error	L^2 rate	H^1 error	H^1 rate	L^2 error	L^2 rate
$\frac{1}{2.5}$	$.1312 \cdot 10^{-2}$		$.5575 \cdot 10^{-2}$		$.1706 \cdot 10^{-2}$	
$\frac{1}{5}$	$.3172 \cdot 10^{-3}$	2.05	$.1638 \cdot 10^{-2}$	1.77	$.6081 \cdot 10^{-3}$	1.48
$\frac{1}{10}$	$.6250 \cdot 10^{-4}$	2.34	$.2798 \cdot 10^{-3}$	2.55	$.1300 \cdot 10^{-3}$	2.23
$\frac{1}{15}$	$.2674 \cdot 10^{-4}$	2.09	$.1437 \cdot 10^{-3}$	1.64	$.5559 \cdot 10^{-4}$	2.10
$\frac{1}{20}$	$.1490 \cdot 10^{-4}$	2.03	$.9515 \cdot 10^{-4}$	1.44	$.3380 \cdot 10^{-4}$	1.73
$\frac{1}{30}$	$.6783 \cdot 10^{-5}$	1.94	$.5815 \cdot 10^{-4}$	1.21	$.2872 \cdot 10^{-4}$	0.40

Table 2.2: Errors of velocity and stress by Crank-Nicolson for $t = 0.4$.

In Table 2.1, the implicit Euler method shows the expected theoretical rate, 1. The Crank-Nicolson method, at the same time, shows higher convergence rates in Table 2.2, and especially the

L^2 errors of the velocity show quadratic convergence. However, we didn't get the expected rate when $\Delta t = \frac{1}{30}$. We suspect the time step Δt is not large enough to dominate the total H^1 error in that case, and this might be why we didn't get the expected rate. However, in the implicit Euler method, the error is expected to be bounded by Δt rather that $(\Delta t)^2$. Hence for the same grid sizes, a certain time step Δt may be large enough to dominate the total error for the implicit Euler method. Therefore, the convergence rates observed in Table 2.1 better match the expected rate.

Test Two

Contrary to Test One, in the second test, we want to investigate how the mesh size would affect the total error of the problem. In order to do that, we fixed the time step Δt by a small enough number so that the finite element discretization error dominates the total error.

We picked a small time step $\Delta t = \frac{1}{2000}$. A sequence of decreasing mesh sizes is used to compute the corresponding errors for velocity and stress, and their respective convergence rates. Table 2.3 and Table 2.4 summarize the numerical results of the implicit Euler and Crank-Nicolson, respectively.

	velocity				stress	
grid	L^2 error	L^2 rate	H^1 error	H^1 rate	L^2 error	L^2 rate
3×3	$.2645 \cdot 10^{-4}$		$.3244 \cdot 10^{-3}$		$.2853 \cdot 10^{-3}$	
5×5	$.8043 \cdot 10^{-5}$	1.72	$.1291 \cdot 10^{-3}$	1.33	$.8307 \cdot 10^{-4}$	1.78
9×9	$.1859 \cdot 10^{-5}$	2.11	$.2477 \cdot 10^{-4}$	2.38	$.1960 \cdot 10^{-4}$	2.08
13×13	$.1139 \cdot 10^{-5}$	1.21	$.1112 \cdot 10^{-4}$	1.98	$.8538 \cdot 10^{-5}$	2.05
17×17	$.9111 \cdot 10^{-6}$	.78	$.7286 \cdot 10^{-5}$	1.47	$.4681 \cdot 10^{-5}$	2.09

Table 2.3: Errors of velocity and stress by Implicit Euler for $t = 0.2$.

Note that the two methods show similar convergence rates since this test is based on a fixed small time step and we expect the total error to be dominated by the spatial discretization. For $h = \frac{1}{16}$ in Table 2.3, the total L^2 error for velocity seems to be affected by a time discretization

	velocity				stress	
grid	L^2 error	L^2 rate	H^1 error	H^1 rate	L^2 error	L^2 rate
3×3	$.2778 \cdot 10^{-4}$		$.3483 \cdot 10^{-3}$		$.3413 \cdot 10^{-3}$	
5×5	$.9417 \cdot 10^{-5}$	1.56	$.1570 \cdot 10^{-3}$	1.15	$.1006 \cdot 10^{-3}$	1.76
9×9	$.1455 \cdot 10^{-5}$	2.69	$.2544 \cdot 10^{-4}$	2.63	$.2172 \cdot 10^{-4}$	2.21
13×13	$.6049 \cdot 10^{-6}$	2.16	$.1230 \cdot 10^{-4}$	1.79	$.1002 \cdot 10^{-4}$	1.91
17×17	$.3916 \cdot 10^{-6}$	1.51	$.6256 \cdot 10^{-5}$	2.35	$.6734 \cdot 10^{-5}$	1.38

Table 2.4: Errors of velocity and stress by Crank-Nicolson for $t = 0.2$.

error. Thus, the time step used may not be small enough to get expected convergence rate. However, we notice that with a relative large grid, 9×9, the convergence rates fit our expectation. In the Crank-Nicolson case, since the error is expected to be bounded by $(\Delta t)^2$ rather than Δt, we obtain a better result with the same grid size.

Chapter 3

Fluid-Structure Interaction Problem

In Chapter 2, the moving boundary of the fluid flow is given by a known function. However, in practice, the time-dependent boundary of a fluid is difficult to describe with a known function. In this chapter, we consider a more realistic interaction problem consisting of a viscoelastic fluid and an elastic tube through which the fluid is moving. This kind of interaction problem has many significant applications in industry and biology. One important application among them is modeling of blood flows in vessels.

In the following work, the deformation of a vessel wall is described by a time-dependent structure equation. The blood flow, whose domain is defined by this moving wall, will be solved by the ALE method introduced in the previous chapter.

3.1 Model description

Our model is based on a portion of fluid defined on a time-dependent domain Ω_t as given in Figure 3.1. S_1 and S_2 represent the upstream and downstream sections, with which the portion we consider is connected to the rest of the vessel.

Considering intersection of the tube, with a vertical plane to simplify the model, we can then have the two-dimensional problem as shown in Figure 3.2. In this simplified case, the inflow

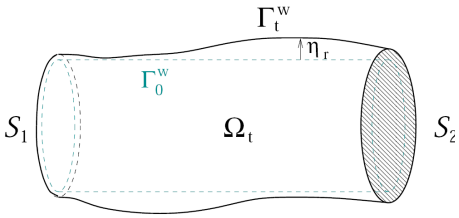

Figure 3.1: Simple compliant tube [23]

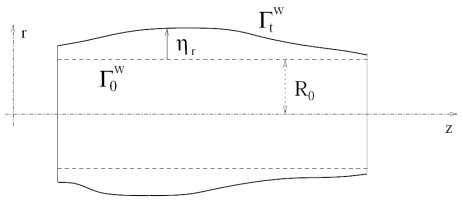

Figure 3.2: Simple compliant tube [23]

and outflow boundaries are denoted by Γ_{in} and Γ_{out}, respectively. What we are more interested in is Γ_t^w, which denotes the time-dependent boundary at time t. In Figure 3.2, Γ_0^w refers to the initial boundary of the fluid. The difference between Γ_t^w and Γ_0^w, denoted by η_r, represents the displacement of the wall and can be described by a structure function.

3.2 Two sub-problem decomposition

In practical applications, to compute the interaction problem, we decompose the whole system into two subproblems: the fluid subproblem and the structure subproblem. Decomposing the system, we can solve two relatively smaller and easier subproblems instead of a big complex one. Using an appropriate decoupling algorithm satisfying certain matching conditions on the interface, we can carry out a simulation for the whole system.

The fluid considered in this interaction system is the viscoelastic fluid flow (2.1)-(2.3). Mathematical notation and the initial conditions used here are the same as in the previous chapter. For the boundary conditions on inflow and outflow boundaries, we consider a Neumann boundary condition which reads as:

$$\begin{cases} (\boldsymbol{\sigma} + 2(1-\alpha)D(\mathbf{u}) - p\mathbf{I}) \cdot \mathbf{n} = g_1 & \text{on } \Gamma_{in} \\ (\boldsymbol{\sigma} + 2(1-\alpha)D(\mathbf{u}) - p\mathbf{I}) \cdot \mathbf{n} = g_2 & \text{on } \Gamma_{out}. \end{cases}$$

Specifically, in the case that $g_2 = 0$, the boundary condition on Γ_{out} describes a natural flow. The condition on Γ_t^w is related to the wall displacement and will be discussed later. Given all the necessary information, similarly to what was discussed in Chapter 2, we can obtain a numerical approximation scheme based on the ALE formulation of the fluid subproblem.

For the structure equation, we consider the one-dimensional *generalized rod model*[28]

$$\rho\frac{\partial^2\eta}{\partial t^2} - a\frac{\partial^2\eta}{\partial z^2} + b\eta - c\frac{\partial^3\eta}{\partial z^2\partial t} = \Phi. \tag{3.1}$$

Here, ρ, a, b, c are all positive parameters that would be given to describe the physical features of the wall tissue. The right hand side function Φ is the forcing term in the radial direction due to the external forces, including the stress produced by the fluid. In fact, it depends on the velocity $\mathbf{u}$ and the pressure p of the blood.

For the boundary condition, the homogeneous boundary conditions $\eta = 0$ at the endpoints $z = 0$ and $z = L$, do not match with reality in the blood flow context. As the structure equation (3.4) is of a propagative type, we consider the first order absorbing boundary conditions [23]

$$\begin{cases} \frac{\partial\eta}{\partial t} - \sqrt{\frac{a}{\rho}}\frac{\partial\eta}{\partial z} = 0 & \text{at } z = 0 \\ \frac{\partial\eta}{\partial t} + \sqrt{\frac{a}{\rho}}\frac{\partial\eta}{\partial z} = 0 & \text{at } z = L. \end{cases}$$

Though the original problem has been split into two subproblem, the fluid problem and structure problem must be carefully connected to each other since they were derived from the whole interaction system. The matching conditions at the moving wall Γ_t^w can be written as:

$$\mathbf{u} = \frac{\partial\eta}{\partial t}\mathbf{n}, \tag{3.2}$$

$$-(\boldsymbol{\sigma} + 2(1-\alpha)D(\mathbf{u}) - p\mathbf{I})\cdot\mathbf{n} = \Phi\mathbf{n}. \tag{3.3}$$

where $\mathbf{n}$ is the outward unit vector to Γ_t^w.

The first matching condition (3.2) guarantees the adherence of the fluid to the structure by making the velocity of the displacement exactly the vertical velocity of the fluid for every point on the interface. The second condition (3.3), according to reaction principle, satisfies the continuity of the stresses on the interface.

The fluid equation is well defined and solvable provided the wall displacement η is available. On the other hand, the structure displacement can be computed when the fluid solution $(\mathbf{u}, p, \boldsymbol{\sigma})$ is given. This is the basic idea of decoupling the whole system from which iterative algorithms may be derived. We discuss an iterative algorithm below.

3.3 Numerical study for the structure

3.3.1 Weak formulation

Consider the structure equation

$$\rho\frac{\partial^2\eta}{\partial t^2} - a\frac{\partial^2\eta}{\partial z^2} + b\eta - c\frac{\partial^3\eta}{\partial z^2\partial t} = \Phi. \tag{3.4}$$

Define $\mathbf{W} := \{H^1(0, L)\}$. Then the weak problem of the structure reads as:
find $\eta \in \mathbf{W}$ such that for all $\xi \in \mathbf{W}$

$$\rho\left(\frac{\partial^2\eta}{\partial t^2}, \xi\right) + b(\eta, \xi) + \left(\left(a\frac{\partial\eta}{\partial z} + c\frac{\partial^2\eta}{\partial z\partial t}\right), \frac{\partial\xi}{\partial z}\right) + \sqrt{\frac{\rho}{a}}\left(a\frac{\partial\eta}{\partial t} + c\frac{\partial^2\eta}{\partial t^2}\right)\xi|_{z=0,z=L} = (\hat{\Phi}, \xi), \tag{3.5}$$

where

$$\hat{\Phi} = \Phi\sqrt{1 + \left(\frac{\partial\eta}{\partial z}\right)^2} \tag{3.6}$$

and Φ is the right hand side of (3.4).

Recall that the matching condition (3.3) is defined on Γ_t^w, hence the term under the square root is introduced due to the change in the surface measure passing from Γ_t^w to Γ_0^w.

3.3.2 Finite element approximation for structure

Define finite element space for the approximation of η:

$$\mathbf{W}_h := \{\eta \in H^1(0, L) : \eta|_k \in P_2(K)\}.$$

The spatial-discretized continuous-in-time formulation is: find $\eta_h \in \mathbf{W}_h$ such that

$$\rho\left(\frac{\partial^2\eta_h}{\partial t^2}, \xi_h\right) + b(\eta_h, \xi_h) + \left(\left(a\frac{\partial\eta_h}{\partial z} + c\frac{\partial^2\eta_h}{\partial z\partial t}\right), \frac{\partial\xi_h}{\partial z}\right) + \sqrt{\frac{\rho}{a}}\left(a\frac{\partial\eta_h}{\partial t} + c\frac{\partial^2\eta_h}{\partial t^2}\right)\xi_h|_{z=0,z=L} = (\hat{\Phi}, \xi_h). \tag{3.7}$$

For the time discretization, we consider the first-order Implicit Euler scheme:

$$\rho\left(\frac{(\eta_h^{n+1},\xi_h)-2(\eta_h^n,\xi_h)+(\eta_h^{n-1},\xi_h)}{\Delta t^2}\right)+b(\eta_h^{n+1},\xi_h)$$
$$+\left(a\frac{\partial\eta_h^{n+1}}{\partial z},\frac{\partial\xi_h}{\partial z}\right)+c\left(\frac{\frac{\partial\eta_h^{n+1}}{\partial z}-\frac{\partial\eta_h^n}{\partial z}}{\Delta t},\frac{\partial\xi_h}{\partial z}\right)$$
$$+\sqrt{\frac{\rho}{a}}\left(a\frac{\eta_h^{n+1}-\eta_h^n}{\Delta t}+c\frac{\eta_h^{n+1}-2\eta_h^n+\eta_h^{n-1}}{\Delta t^2}\right)\xi_h|_{z=0,z=L}=(\hat{\Phi},\xi_h). \quad (3.8)$$

3.4 Coupled algorithm

So far, we have illustrated how to decompose the interaction problem into two subproblems, and we have developed a numerical method for each. To simulate the whole system, we must find an appropriate algorithm to connect the two solvers. Various implicit or explicit algorithms can be applied to this coupled problem. In this paper, we considered the *first order explicit algorithm* (also called the *loosely coupled scheme*). The algorithm is presented in figure 3.3.

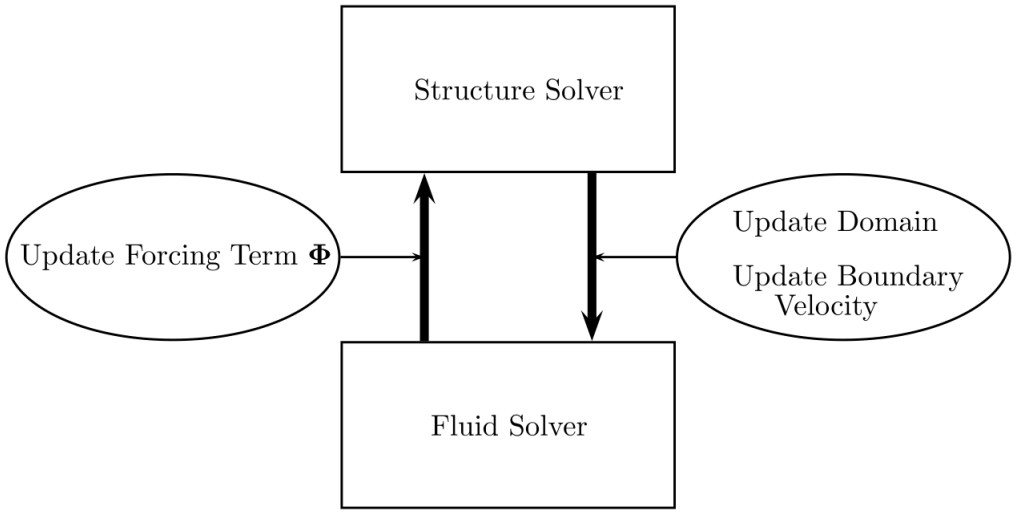

Figure 3.3: Explicit coupled algorithm

As illustrated, in this algorithm the structure can be solved in advanced time, providing a new

boundary position and boundary velocity for the fluid, since its forcing term Φ is determined by $(\mathbf{u}^n, p^n)$ from the previous time step. The two subproblems communicate with each other by two matching conditions, one is the forcing term on the wall due to the fluid and the other is the boundary value of the fluid given by the velocity of the displacement of the wall. This simple splitting algorithm is often known as the *conventional serial staggered scheme (CSS)*.

To state what was illustrated in figure 3.3 more clearly, we summarize the algorithm as follows:
In each time interval $[t_n, t_{n+1}]$

1. Solve the structure equation using the forcing term obtained from the previous time level t_n.

2. Update the domain, the boundary velocity of the fluid, and the ALE mapping. For each point (x, y) on the boundary, a new position of the boundary at time step $n+1$ can be computed as

$$x_{(n+1)} = x_0, \tag{3.9}$$

$$y_{(n+1)} = y_0 + \eta_{(n+1)}. \tag{3.10}$$

   The boundary velocity for the fluid is computed by a finite difference scheme and the ALE mapping is computed by the harmonic expression.

3. Solve the fluid equations in the updated domain Ω_{n+1}. By the ALE method discussed in previous chapter, we compute $(\mathbf{u}_{n+1}, p_{n+1}, \boldsymbol{\sigma}_{n+1})$.

4. Compute the forcing term Φ of the structure equation by (3.3) using $(\mathbf{u}_{n+1}, p_{n+1}, \boldsymbol{\sigma}_{n+1})$.

Comparing this to other schemes, the explicit algorithm has an advantage in efficiency, since for each time step, it only requires one-time solving of each subproblem.

3.5 Numerical test

In this section, we illustrate some numerical results obtained by applying the algorithm discussed in the previous section.

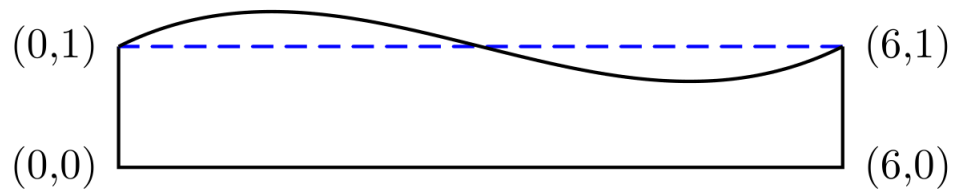

Figure 3.4: Model for numerical experiment

The figure 3.4 shows a domain considered for numerical tests. Suppose both the fluid and structure are started from rest. A rectangle of height $D = 1$ and length $L = 6$ is defined as the initial domain for the fluid flow. Without losing generality, we may suppose that the bottom boundary of the domain is a fixed wall and the top edge is deformable in the vertical direction.

On the inflow and outflow boundaries, we consider a Neumann boundary condition for the fluid. More precisely, the boundary condition imposed on the inflow section is

$$(\boldsymbol{\sigma} + 2(1-\alpha)D(\mathbf{u}) - p\mathbf{I}) \cdot \mathbf{n} = \begin{cases} 10^4[\cos(\frac{\pi t}{2.5ms}) - 1]\mathbf{n} & 0 \le t \le 5 \\ \mathbf{0} & 5 < t < T \end{cases},$$

while on the outflow section

$$\boldsymbol{\sigma} + 2(1-\alpha)D(\mathbf{u}) - p\mathbf{I}) \cdot \mathbf{n} = \mathbf{0}.$$

For the fluid equations, the parameters are set as $\alpha = 0.5, \quad \lambda = 0.5, \quad \rho = 50$. The parameters for the structure equation are $a = 25000, \quad c = 0.01, \quad b = 400000$.

For the spatial discretization, we consider (P_2, P_1, P_{1DG}) for the fluid equation and P_2 finite elements for the structure. The Implicit Euler Method is applied for time discretization to both the fluid and structure subproblems.

The numerical experiment was based on a 5×25 uniform grid mesh initially and remeshed according to the ALE mapping. A time step $\Delta t = 0.0046$ was used. Figures (3.5)-(3.9) illustrate the displacement of the wall at varies $t = 0.09, 0.23, 0.32, 0.46, 0.69$, respectively. For comparison, we

performed similar numerical tests for a Newtonian fluid-structure problem based on the same mesh size and time step. These two problems share the same parameters with the exception of the value of λ. We set $\lambda = 0.5$ for the viscoelastic fluid and $\lambda = 0$ for the Newtonian case. In each figure, the solid curve represents the configurations of the wall for the non-Newtonian case, while the dashed curve represents the Newtonian case.

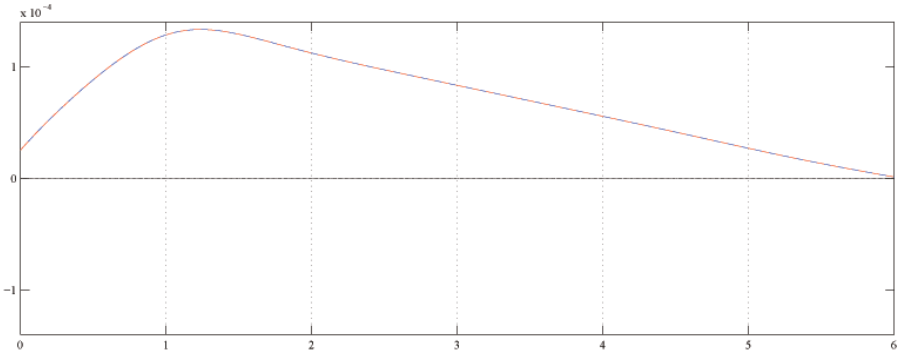

Figure 3.5: Displacement of the wall at t=0.09

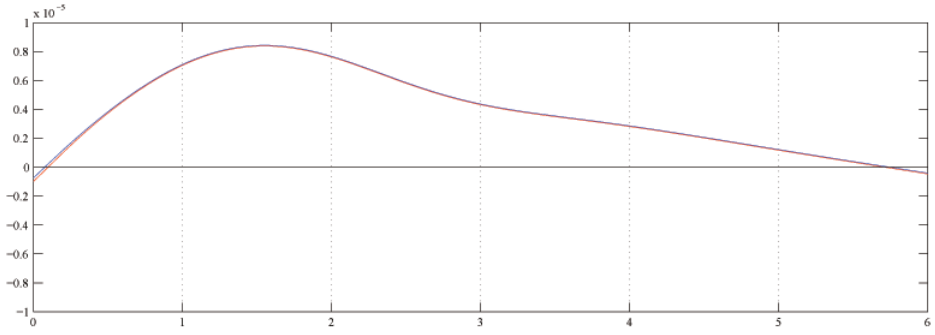

Figure 3.6: Displacement of the wall at t=0.23

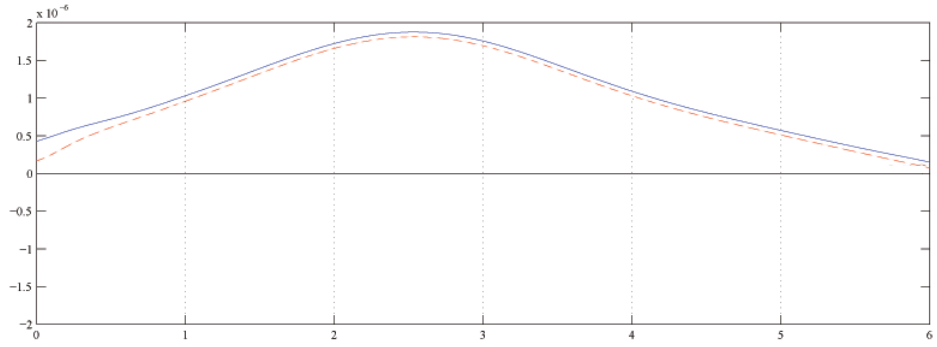

Figure 3.7: Displacement of the wall at t=0.32

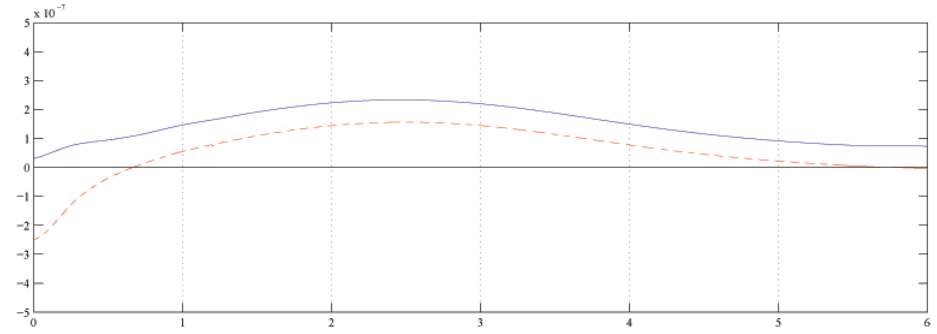

Figure 3.8: Displacement of the wall at t=0.46

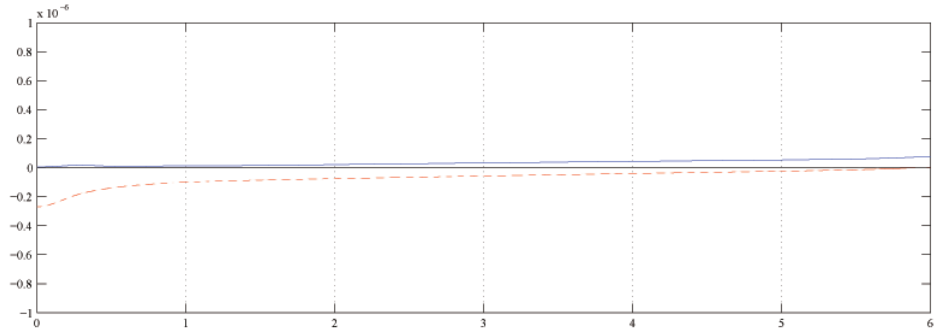

Figure 3.9: Displacement of the wall at t=0.69

From the above figures, we may observe the presence of a smooth wave inside the tube, which matches our expectation on the motion of the fluid. More precisely, we observe a bump moving horizontally from the inflow section to the outflow section. The magnitude of the summit value does not blow up in the procedure. The configuration went back to zero after a certain time since the force imposed on the inflow section is set to be zero after 5ms in (3.5). Hence, the fluid depicted by the sequence of figures match the physical meaning of our numerical experiment.

At the same time, we may observe that the gap between the Newtonian and the non-Newtonian curves increases as time goes (it can be negligible in first two figures). This difference suggests that using a Newtonian model in blood flow simulation may lead to significant modeling and numerical errors.

However, we found that the explicit coupling algorithm was not stable enough over a long period. The numerical result show significant instability and dramatic oscillation if the mesh size and time step are not carefully picked. In fact, the explicit coupling algorithm seems relatively more stable for Newtonian fluid than non-Newtonian ones.

Chapter 4

Conclusions and Future work

In this thesis, we discussed a finite element method for solving a viscoelastic fluid in a moving domain, based on the ALE. Several numerical experiments were presented to test convergence rates for two different time discretization methods: implicit Euler and Crank-Nicolson methods. Then we extended our discussion to a fluid-structure interaction problem. We showed how to decompose the problem into two subproblems, and investigated a numerical method for the structure subproblem. A staggered explicit algorithm was used as a time stepping scheme and numerical results of the algorithm were presented.

The explicit algorithm is appealing in terms of efficiency (compare to an implicit algorithm), and it can be used to simulate the fluid-structure system in some cases. However, we found out that this algorithm is not stable for a long time period. Therefore we are going to investigate several other stable algorithms for the fluid-structure interaction problem in the future. In addition, we will extend the 2D-1D problem considered here to a 2D-2D case.

Bibliography

[1] J. Baranger and D. Sandri, Finite element approximation of viscoelastic fluid flow: Existence of approximate solutions and error bounds I. Discontinuous constraints, *Numer. Math.*, 63, 13-27, 1992.

[2] T. Bodnár and A. Sequeira, Numerical study of the significance of the non-Netwonian nature of blood in steady flow through a stenosed vessel, *Advances in Mathematical Fluid Mechanics*, Springer, 83-104, 2010

[3] T. Bodnár, A. Sequeira, and M. Prosi, On the shear-thinning and viscoelastic effects of blood flow under various flow rates, *Appl. Math. Comput.*, 217, 5055-5067, 2011.

[4] D. Boffi and L. Gastaldi, Stability and geometric conservation laws for ALE formulations, *Comput. Methods. Appl. Mech. Engrg.*, 193, 4717-4739, 2004.

[5] S. Canić, A. Mikelić, and J. Tambaca, Two dimensional effective model describing fluid-structure interaction in blood flow: analysis, simulation and experimental validation, Comptes Rendus Mechanique Acad. Sci., 333, 867-883, 2005.

[6] Y.C. Chang, T.Y. Hou, B. Merriman, and S. Osher. A level set formulation of eulerian interface capturing methods for incompressible fluid flows.*J. Comput. Phys.*, 124(2), 449-464, 1996.

[7] P. Causin, J-F. Gerbeau and F. Nobile, Added-mass effect in the design of partitioned algorithms for fluid-structure problems, *Comput. Methods Appl. Mech. Engrg.* 194, 4506-4527, 2005.

[8] J. Donea, S. Giuliani, J.P. Halleux, An arbitrary Lagrangian-Eulerian finite element method for transient dynamic fluid-structure interactions, *Comput. Methods Appl. Mech. Engrg.*, 33, 689-723, 1982.

[9] L. Formaggia, J.F. Gerbeau, F. Nobile, A. Quarteroni, On the Coupling of 3D and 1D Navier-Stokes equations for Flow Problems in Compliant Vessels, *Comput. Methods Appl. Mech. Engrg.*, 191, 561-582, 2001.

[10] L. Formaggia and F. Nobile, A stability analysis for the arbitrary Lagrangian Eulerian formulation with finite elements, *East-West J. Numer. Math.*, 7, 105-131, 1999.

[11] L. Formaggia, A. Quarteroni, and A. Veneziani. Cardiovascular mathematics: Modeling and simulation of the circulatory system, volume 1 of *MS&A. Model. Simul. Appl.*, Springer Italia, Milan, 2009.

[12] L. Formaggia, A. Moura and F. Nobile, On the stability of the coupling of 3D and 1D fluid-structure interaction models for blood flow simulations, *Math. Mod. Numer. Anal. (M2AN)*, 41, 743-769, 2007.

[13] T.J.R. Hughes, W.K. Liu and T.K. Zimmermann, Lagrangian-Eulerian finite element formulation for incompressible viscous flows, *Comput. Methods. Appl. Mech. Engrg.*, 29, 329-349, 1981.

[14] J. Janela, A. Moura, and A. Sequeira, A 3D non-Newtonian fluid-structure interaction model for blood flow in arteries, *J. Comput. Appl. Math.*, 234, 2783-2791, 2010.

[15] W. Layton, *Introduction to the numerical analysis of incompressible viscous flows*, SIAM, Philadelphia, 2008.

[16] H. Lee, A multigrid method for viscoelastic fluid flow, SIAM *J. Num. Anal.*, 42, 109-129, 2004.

[17] H. Lee and A. Liakos, Two-level finite element discretization of viscoelastic fluid flow *Comput. Methods. Appl. Mech. Engrg.*, 192, 4965-4979, 2003.

[18] M. Lukáčová and A. Zauškozá, Numerical modelling of shear-thinning non-Newtonian flows in compliant vessels, *Int. J. Numer. Meth. Fluids*, 56, 1409-1415, 2008.

[19] H. Lee, Numerical approximation of Quasi-Newtonian flows by ALE-FEM, to appear *Numer. Methods PDE*, 2011.

[20] J.S. Martin, L. Smaranda and T. Takahashi, Convergence of finite element/ALE method for the Stokes equations in a domain depending on time, *Journal of Computational and Applied Mathematics*, 230, 521-545, 2009.

[21] A. Masud and T.J.T.Hughes. A space-time galerkin/least squares finite element formulation of the Navier-Stokes equations for moving domain problems *Comp. Meth. Appl. Mech. Engrg.*, 146, 91-126, 1997.

[22] L. Nadau and A. Sequeira, Numerical simulations of shear dependent viscoelastic flows with a combined finite element–finite volume method, *Comput. Math. Appl.*, 53, 547-568, 2007.

[23] F. Nobile, *Numerical approximation of fluid-structure interaction problems with application to haemodynamics*, Ph.D. thesis, 2001.

[24] F. Nobile and C. Vergara, An effective fluid-structure interaction formulation for vascular dynamics by generalized Robin conditions, *SIAM J. Sci. Comp.*, 30, 731-763, 2008.

[25] R.G. Owens and T.N. Phillips, *Computational rheology*, Imperial College Press, London, 2002.

[26] C.S. Peskin. Numerical Analysis of Blood Flow in the Heart. *J. of Comput. Phys.*, 25, 220-252, 1977.

[27] C.S. Peskin.and D.M. McQueen. A Three Dimensional Computational Method for Blood Flow in the Heart-I Immersed Elastic Fibers in a Viscous Incompressible Fluid. *J. Comput. Phys.*, 81(2), 372-405, 1989.

[28] A. Quarteroni, M. Tuveri and A. Veneziani, Computational vascular fluid dynamics: problems, models, and methods, *Comput. Visual Sci.*, 2, 163-197, 2000.

[29] T.E. Teaduyar, M.Behr, and J.Liou. A new strategy for finite element computations involving moving boundaries and interface-the deforming-spatial-domain/space-time procedure: I. the concept and preliminary numerical tests *Comp. Meth. Appl. Mech. Engrg.*, 94, 339-351, 1992.